Using Laser Assisted Drilling Method with MPD and UBD Condition In Case Of Geothermal Resources

Bazargan Mohsen[1,2], Gudmundsson Agust[1], Meredith Philip[2].

[1] Royal Holloway University of London, Earthscience department, Egham, Surrey, UK

[2] University College London, Earthscience department, London, London, UK

Mohsen.Bazargan.2014@live.rhul.ac.uk

Keywords: Underbalanced drilling, managed pressure drilling, thermal operation, plasma torch.

ABSTRACT

Investigation of the wellbore instability induced by the application of plasma torch as a thermal assisted drilling and completion in carbonated reservoirs and transfer this method to geothermal industry is discussed. By using developed theory of elasticity the stresses and strains around the borehole are computed. Consequently, the wellbore instability analysis of thermal assisted drilling in Managed Pressure Drilling (MPD) and Underbalanced Drilling (UBD) is given with a proper drilling fluid. It is found that to evaluate the possibility of the wellbore instability in focusing on the effect of heat transfer some necessary regulations should be fulfilled. This work also mentioned on laboratory experiments of plasma torch interactions and rock texture. Limestone, Granite and Shale samples interact with temperature that generated from plasma torch with initiating and propagation fractures.

1. INTRODUCTION

In recent years, problems associated with drilling oil and gas wells around the large urban circumstances had become the actual limitation of the underground drilling and damages on environments in highly populated or industrialized areas. Therefore, the development of underground drilling mechanism has highly focused [1-6]. Hard rock drilling is an expensive process due to the fact that drill string machines and bottom hole assembly must be extremely rugged and powerful to overcome the intact hard rocks [3-10]. In the presented method to assist improving the hard rock drilling machines, this is achieved by developing techniques to weaken the rock before it is mechanically removed [9-12]. This is obtaining by generating uniform holes inside of rock texture during drilling and perforation operation [10-13]. Recently it is reported that making of holes inside the intact rocks may not be a suitable method [9-12]. It is proposed that a proper method to change the hard rock into a loss rock can be achieved by generating fractures into the rock texture [10-13]. The fractures can be generated with transferring a high temperature gradient with the rock. Temperature can cause expansion and eventually breakdown in many situations by effective expansion. One way to induce a proper temperature is using plasma torch in order to assist the drilling operation. During thermal assisted drilling operation fractures are generated inside of the wellbore and this can reduce the wall strength considerably [19-20]. Plasma arc torch can generated that temperature into the rock and material texture [30-34].

Thermal operation requires air or water drilling fluid. Therefore instead of conventional drilling methods in carbonate reservoir it is necessary to use, other methods of drilling such as UBD and MPD. UBD operation is a drilling condition in which the hydrostatic head of mud column is maintained at a pressure less than that of fluid in the porous medium [1-10]. Although the differences between the medium pore pressure and mud column pressure can cause to flowing the fluid into the wellbore; however, the resulted kick must be under control. Formation damage caused by mud invasion in Overbalanced drilling (OBD) can be avoided in MPD and UBD [1-10]. The MPD and UBD can decline the amount of lost circulation, minimize differential sticking, increase drilling rate and finally lead to higher productivity completions due to minimization of the formation damage [14-16].

In this paper we focus on the thermal assisted MPD and UBD operations, emphasizing the stability of borehole and feasibility of these methods for the future rescue operations such as casing design. Underbalanced drilling has been an appealing idea for drilling engineers since invention when they started to think of it as a novel method to mitigate drilling problems by reducing prospective formation damage to the oil fields e.g. Skin effects. In the experimental part of this work the rock mechanical and thermal approaches are performed and discussed in the following.

2. EXPERIMENTAL WORKS

In this work two separate experimental set up is used with completely divided scientific issues, namely rock mechanical and thermal approaches. In rock mechanical tests, we prepared samples with the standard size of uniaxial test. Using six similar rock samples prepared for uniaxial test the elasticity modulus, Poisson ratio are determined and shown in Table1.

Table1: Material properties

Material	**E** (GPa)	poison ratio	**D** (mm)	**H** (mm)
Limestone	11	0.25	54	108
Granite	38	0.25	54	108
Shale	1.2	0.25	54	108

In material test laboratory we managed to get following data for our rock samples. This heat transfer related parameters are shown in Table 2. The plasma source used in this work is a thermal plasma model which creates effective plasma and the related nozzle produces 1.8 inch heat flam. Fig. 1 shows the experimental arrangement in which the compressed air is used for the 2 Kw plasma torch. The idea of usage the plasma torch is related to the high power jet machine and welding industry. In these above industries plasma torch reported that it is capable of vaporizing and melting the high strength materials such as steel [18-22].

In using an electric arc various parameters should be considered including the magnet fields and gas flow. The chamber materials are also important in confining the arc such as the elements which are usually under high electric voltage [23-25].

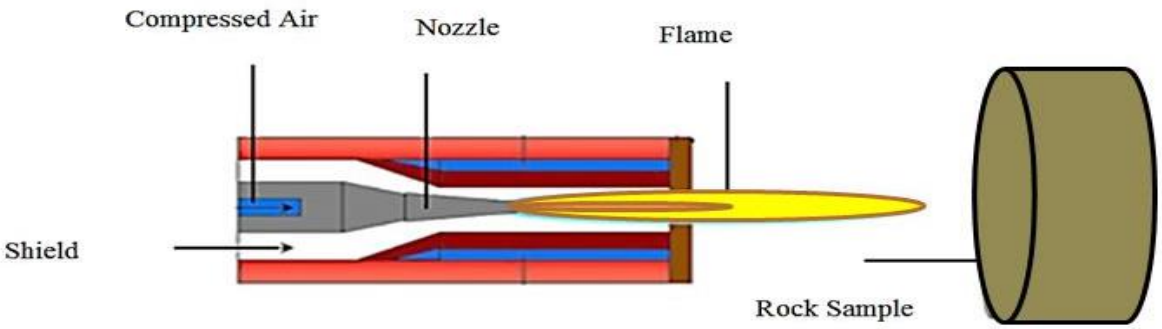

Figure y: This is a figure caption, bold, 6 pt space before and 9 pt space after, indented from the second line on by 0.95 cm.

Table2: mechanical properties of specimens

	limestone	granite
thermal conductivity	1.26	1.33
density	2700	2750
heat transfer coefficient	1.1	1.1
specific heat	0.908	0.908
thermal expansion	1.90E-06	2.55E-06
bulk density	2.65	2.71
diffusivity and thermal inerta	45	45
heat generation rate	0.78	0.83
vaporizing point	2471	3400

3. Governing porous medium equations

The rock sample specimen this research group works on is a known as a rock with specific porosity and permeability which is saturated with fluids. In the beginning, equations had been drive and being discrete with the finite element method (FEM). After that, to make them work on dynamic examples in these equations being discrete again in time and then new source code generates in MATLAB for different examples. To solve dynamic non single phase problems, solid state and pore fluid interactions should be considered. For this reason, owing the fact that porosity definition is total volume minus volume of solid state and also considers that the main source of rock deformation is effective stress rather than pore fluid pressure [ref 1-27 hg]. Moment balance

equations and mass balance for saturated medium had been made and they should be couple to work for this case.

2.1. Moment Balance Equations

Moment balance equation for each phase is like [ref2-19-kh] equation (1):

$$\nabla.\boldsymbol{\sigma}_{\pi} + \rho_{\pi}\mathbf{b} - \rho_{\pi}\ddot{\mathbf{u}}_{\pi} = 0 \qquad (1)$$

In this equation $\boldsymbol{\sigma}$ is matrix stress, ρ_{π} is density of each phase, $\mathbf{b}$ is gravitational acceleration $\ddot{\mathbf{u}}_{\pi}$ is acceleration of specific phase.

This equation should be write and driven for each phase and couple them together with their porosity proportion. By ignoring the effect of velocity difference of solid state and fluid state on account of the fact that this is relatively small, then the main moment balance equation for this medium is as follow:

$$\nabla.\boldsymbol{\sigma} + \rho\mathbf{b} - \rho\ddot{\mathbf{u}} = 0 \qquad (2)$$

In above equation ρ is a mean density and it can be generated from equation (3):

$$\rho = (1-n)\rho_f + n\rho_s \qquad (3)$$

2.2. Mass balance Equation

Mass balance (continuity) equation for each phase in as follow [ref2-19-kh] equation (4):

$$\frac{\partial \rho_{\pi}}{\partial t} + \nabla.(\rho_{\pi}\mathbf{v}_{\pi}) = 0 \qquad (4)$$

In above equation $\mathbf{v}$ is the velocity of each specific phase. Just like the last section, this equation should be written and driven for each phase and couple them together with their porosity proportion. Also Fernandez [ref3-20-kh] writes the fluid density changes equation under temperature and pressure as follow:

$$\rho_f = \rho_{f0}\exp[-\beta_f T + \frac{1}{K_f}(p - p_0)] \qquad (5)$$

By put above equation in the main equation we can generate new equation for mass balance in the form of (6):

$$\nabla^T[\mathbf{k}(-\nabla P + \rho_f \mathbf{g})] + \frac{\dot{p}}{Q^*} = 0 \qquad (6)$$

And in this equation **k** is a permeability matrix, g earth gravitational constant, p is pressure, ρ_f is fluid density and Q^* is a parameter that depends on volume of fluid (K_f) and solid (K_s) and porosity:

$$\frac{1}{Q^*} = \frac{1-n}{K_s} + \frac{n}{K_f} \qquad (7)$$

Now all these equations should be discreted by FEM and they should be written in matrix forms (8) and (9):

$$\mathbf{M}\ddot{\bar{\mathbf{u}}} + \mathbf{K}\bar{\mathbf{u}} - \mathbf{Q}\bar{\mathrm{p}} = \mathbf{f}_1$$

,

$$\mathbf{M} = \int_{\Omega} \mathrm{N}^T \rho \mathrm{N} d\Omega$$

$$\mathbf{K} = \int_{\Omega} \mathbf{B}^T \mathbf{D}\mathbf{B} d\Omega$$

$$\mathbf{Q} = \int_{\Omega} \mathbf{B}^T \mathbf{m}\mathrm{N} d\Omega$$

$$\mathbf{f}_1 = \int_{\Gamma} \mathrm{N}^T \mathbf{t} d\Gamma + \int_{\Omega} \mathrm{N}^T \rho \mathbf{b} d\Omega \qquad (8)$$

$$\mathbf{Q}^T\dot{\bar{\mathbf{u}}} + \mathbf{H}\bar{\mathrm{p}} + \tilde{\mathbf{S}}\dot{\bar{\mathrm{p}}} = \mathbf{f}_2$$

,

$$\mathbf{Q}^T = \int_{\Omega} N^T \mathbf{m}\mathbf{B} d\Omega$$

$$\mathbf{H} = \int_{\Omega} (\nabla N)^T \mathbf{k} \nabla N d\Omega$$

$$\tilde{\mathbf{S}} = \int_{\Omega} (N)^T \frac{1}{Q^*} N d\Omega$$

$$\mathbf{f}_2 = \int_{\Gamma} \mathrm{N}^T q_f d\Gamma + \int_{\Omega} (\nabla N)^T (\mathbf{k}\rho\mathbf{g}) d\Omega \qquad (9)$$

In above relations, N is the shape function, **B** is the derivatives of shape functions, **D** is the material

property of solid skeleton and **m** is the vector of Dirac delta function.

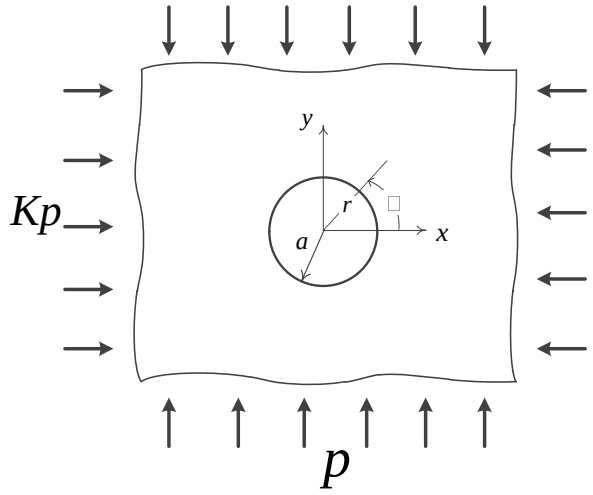

Fig2. Plain stress scheme of presenting analytical equations

Finally, these equations will be discrete in time by newmark method [28hg]. In this method, by coupling equations (8) and (9), the output will be pressure and displacement. To clarify the experimental steps, affected area should be investigated by a suitable modeling. Fig. 2 shows the modeled wellbore by an infinite medium in the $x-y$ plain which contains a circular opening with radius a at its center and subjected to a uniform far-field pressures P and K_p in vertical and horizontal directions, respectively. Note that dimension of the media in the Z direction is very large; hence it is assumed to be in plain strain condition. The distribution of the stress and displacement around the circular openings are explicitly expressed by the *Kirsch* solution borrowed from classical theory of elasticity developments as [26]:

$$\sigma_{rr} = \frac{P}{2}[(1+K)(1-\frac{a^2}{r^2}) - [(1-K)(1-4\frac{a^2}{r^2}+\frac{a^4}{r^4})\cos 2\theta)]] \tag{10}$$

$$\sigma_{\theta\theta} = \frac{P}{2}[(1+K)(1-\frac{a^2}{r^2}) - [(1-K)(1+\frac{a^4}{r^4})\cos 2\theta]] \tag{11}$$

$$\sigma_r = \alpha E \frac{1}{b^2}\int_0^r Trdr + \frac{E}{1-\nu^2}\left[-(1+\nu)^2\,\alpha\frac{1}{b^2}\int_0^b Trdr\right]$$
$$+\alpha E\left[-\frac{(1+\nu)^2}{(1-\nu)}\alpha\frac{1}{b^2}\int_0^b Trdr - \frac{1}{r^2}\int_0^r Trdr\right] \tag{12}$$

$$\sigma_\theta = \alpha E \frac{1}{r^2}\int_0^r Trdr - \alpha ET + \frac{E}{1-\nu^2}\left[-(1+\nu)^2\,\alpha\frac{1}{b^2}\int_0^b Trdr\right]$$
$$+\alpha E\left[-T - \frac{(1+\nu)}{(1-\nu)}\frac{1}{r^2}\int_0^b Trdr - \frac{1}{r^2}\int_0^r Trdr\right] \tag{13}$$

$$\tau_{r\theta} = \frac{P}{2}[(1-K)(1+2\frac{a^2}{r^2}-3\frac{a^4}{r^4})\sin 2\theta] \tag{14}$$

$$u_r = -\frac{Pa^2}{4Gr}[(1+K)-(1-K)(4(1-\nu)-\frac{a^2}{r^2})\cos 2\theta] \tag{15}$$

$$u_\theta = -\frac{Pa^2}{4Gr}[(1-K)(2(1-2\nu)+\frac{a^2}{r^2})\sin 2\theta] \quad (16)$$

In which r and θ are the polar coordinates, σ_r and σ_θ are thermal stresses and the others are related to in-situ stresses. E and ν are denote to the elastic modulus and poison's ratio, respectively. The above mentioned equations are used in the present work to calculate the stresses and displacement contours in the following [26].

3.2. Analytical Modeling

In this part we are presenting two different analytical modeling with Mathematica software to present wellbore instability and also thermal stresses around the borehole. In the first model we use equation 10, 11, 15 and 16. With these analytical equations we want to present displacement and stresses around wellbore to present stable situation and instable situation in three very simple models. Figure3 is basically showing principal stresses and total displacement in underbalanced condition when drilling fluid pressure is less than pore pressure plus in place principal stresses. Figure4 is showing over balanced condition when drilling fluid pressure is more than pore pressure plus in situ stresses. In figure5 we present how managing this pressure work and how stable situation will basically should work in ideal condition. We calculate and analysis how to make balance between inside and outside pressures.

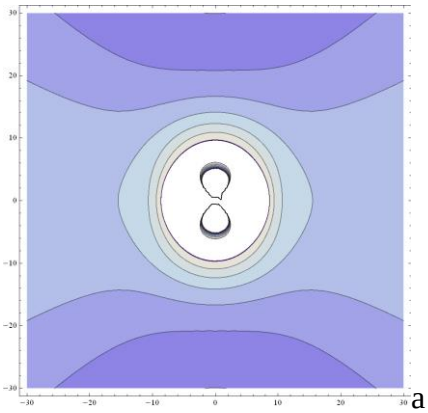
a

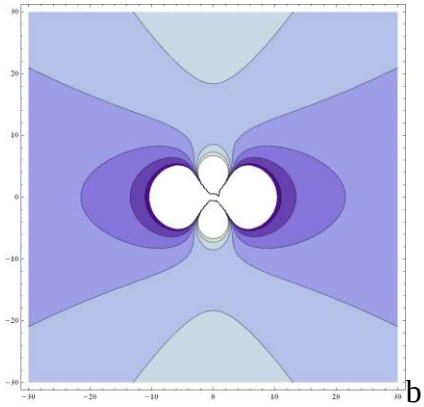
b

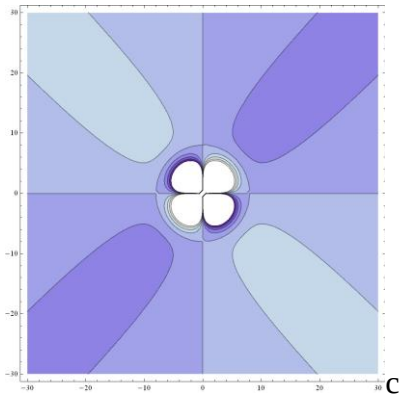
c

Figure3: a) first principal stress b) third principal stress and c) is total displacement in underbalanced condition

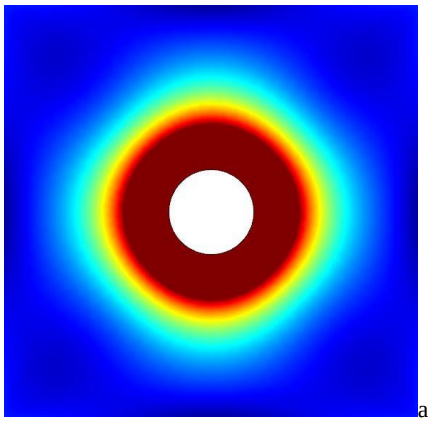
a

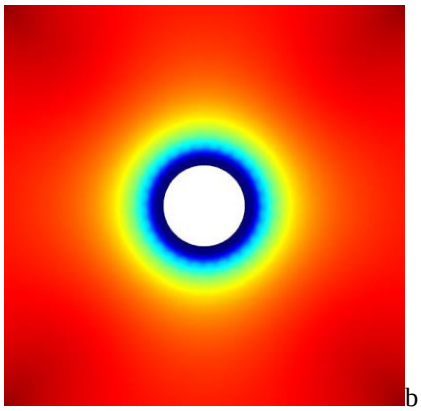
b

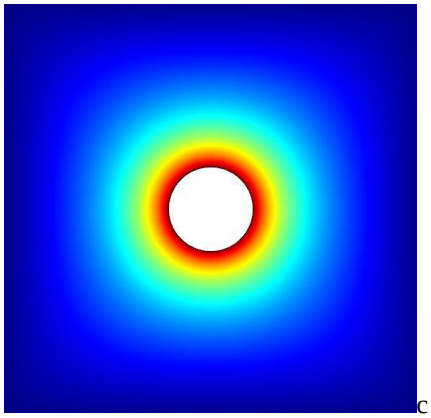
c

Figure4: a) first principal stress b) third principal stress and c) is total displacement in overbalanced condition

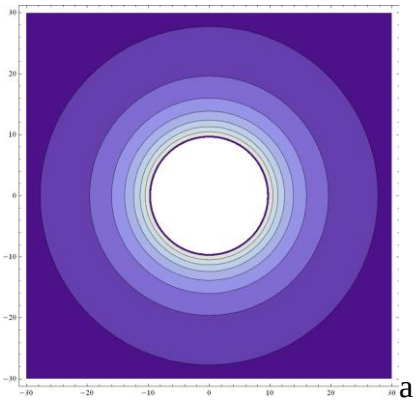

Figure5: a) first principal stress b) third principal stress in managing this pressure and stable condition

Second model is all about thermal stresses. This model had been run for three different rocks under same temperature. In this work we present thermal stresses that can be generated and effect rock body. All rock properties are from table1 and table2. Figure6 is the Granite sample, Figure7 is limestone and Figure 8 is Shale under the same temperature. Heat source of all of them were plasma torch. The temperature generated out of that setup were calculate and it is been using for these following modeling.

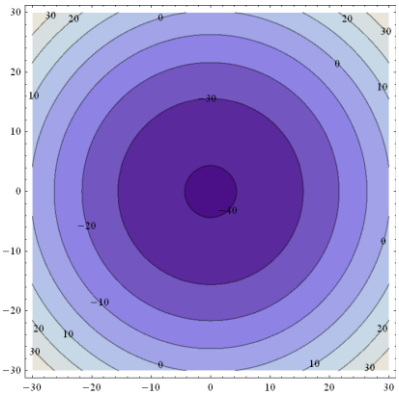

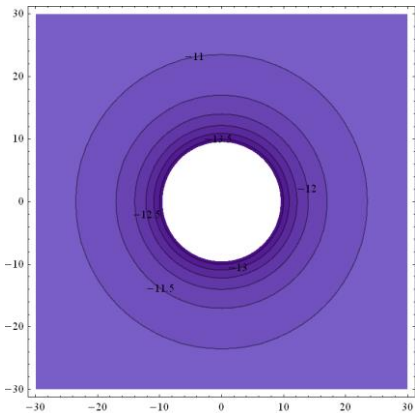

Figure6: Granite sample under 1900 Celsius degree

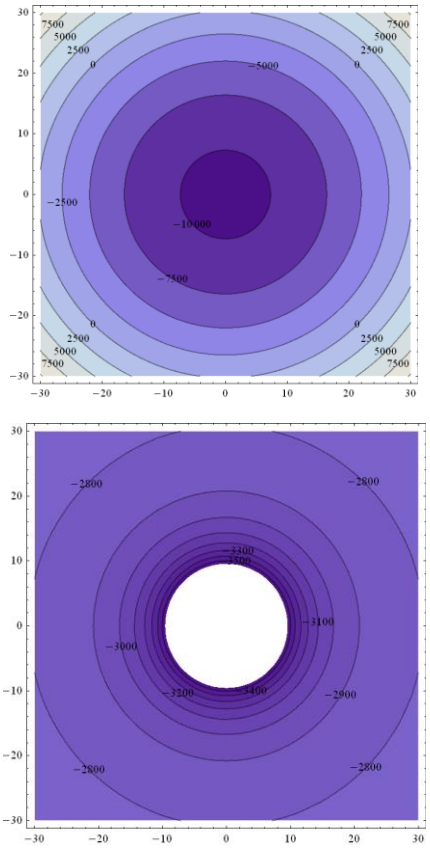

Figure7: Limestone sample under 1900 Celsius degree

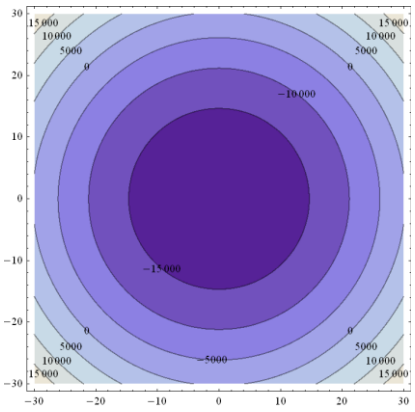

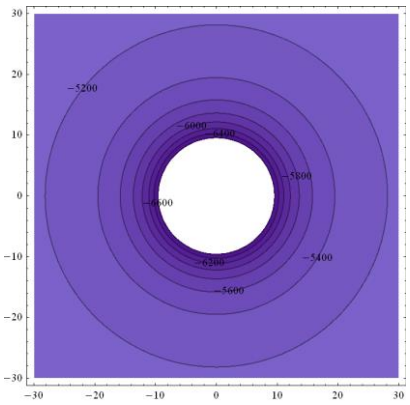

Figure8: Shale Granite sample under 1900 Celsius degree

3.3. Finite Element Modeling

In this section we consider on thermal stress creation and their effect on our specimen during plasma arc operation. For this reason, we prepare specimens for this experiment with initial cracks and without initial cracks. In samples with mechanical properties in table-1 and table-2 were modeled by using finite element method in COMSOL software. Stress concentration in cause by this heat transfer inside of sample had shown with case of sample with or without crack. In this section we are going to simulate one example and this example has different sections. First example has included three different sections. In the first section we present intact rock under the temperature of plasma torch. As you can see in this figure9 the specimen was under plasma torch heat convention and this induced temperature caused displacement. This sample without any natural crack used for plasma operation and the process was simulated stationary in the software. Next section of this example is presenting same rock sample with -45 degree angled crack close to the center of the rock. Crack has introduced as empty cavity and the center of the rock is the main contact area between rock and plasma torch flam. In figure10 it has shown how thermal stresses which were generated from plasma torch affecting on same granite sample under the same condition. The only difference is the one natural fracture close to the plasma interaction spot. How this empty cavity interact with thermal stresses and how these stresses can force this crack to propagate in shown direction. Next part of this example is more difficult and interesting than the others. In this part we simulating limestone sample with four initial fractures. Fractures define as empty cavity in this example and they have been presented in four different angels. They have 45, -45, 0 and 90 degrees. In this example we are trying to show thermal stresses around these fractures and how they are going to go propagating during plasma torch experiment tests. Figure11 shows how the heat transfer in rock surface and how this heat can cause displacements in surface and stresses around cracks.

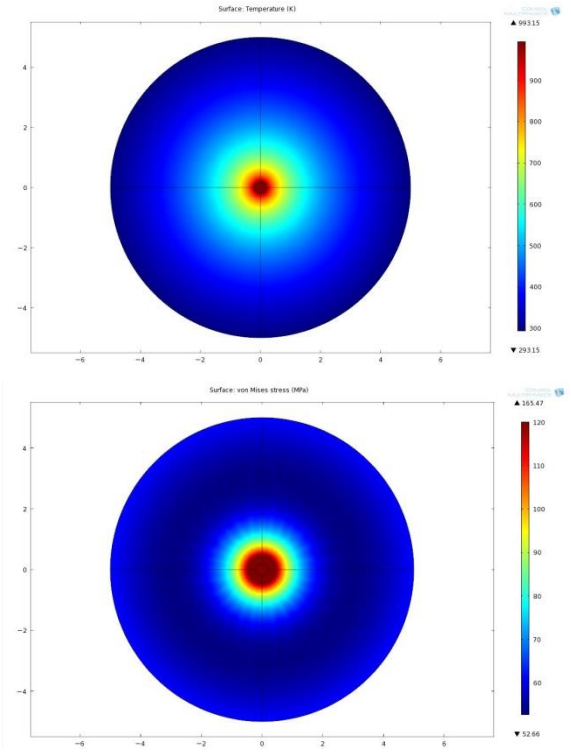

Figure9: granite without fracture under plasma arc interaction

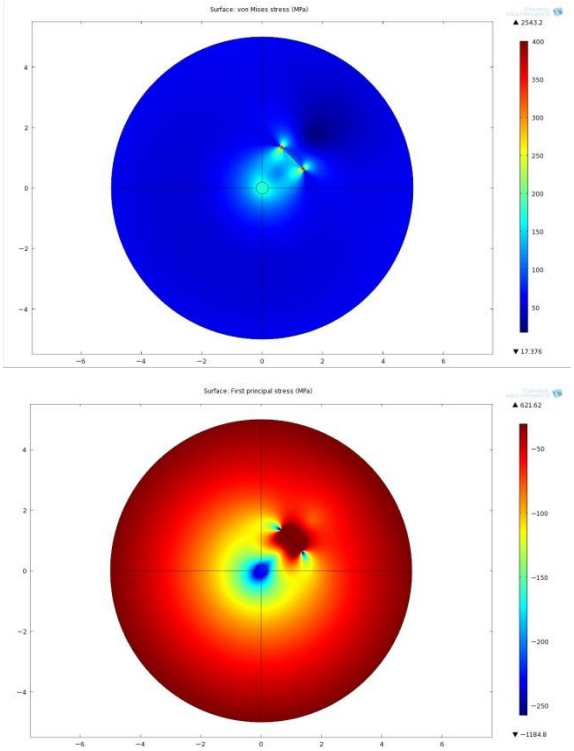

Figure10: a) contour of von-mises b) displacement during plasma arc interaction granite with natural fracture under plasma arc interaction

Figure 11: Experimental result of Limestone uder plasma torch test. Damages and fractures are macroscopic and visible.

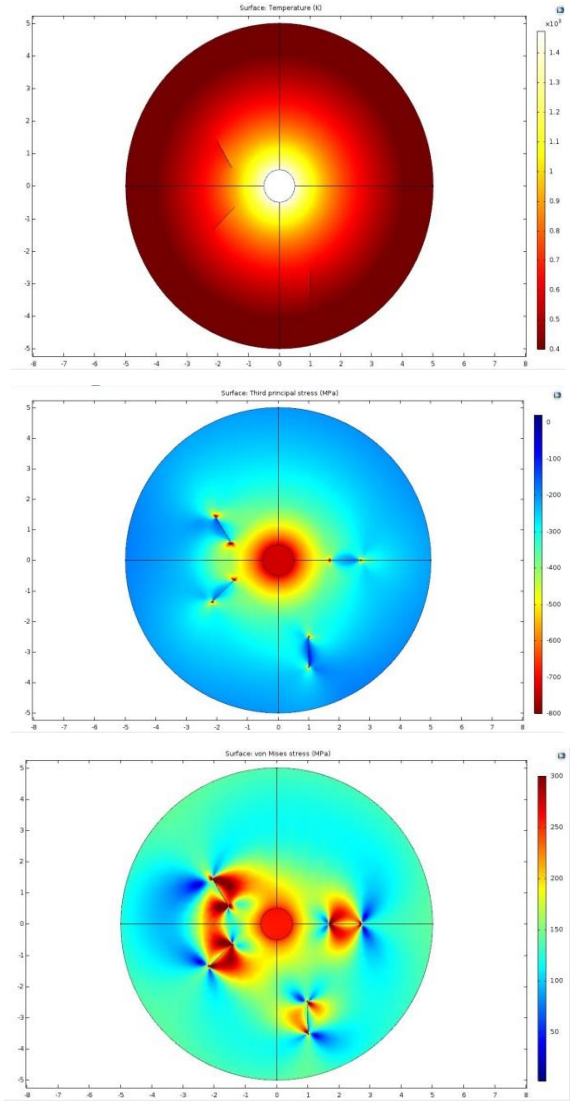

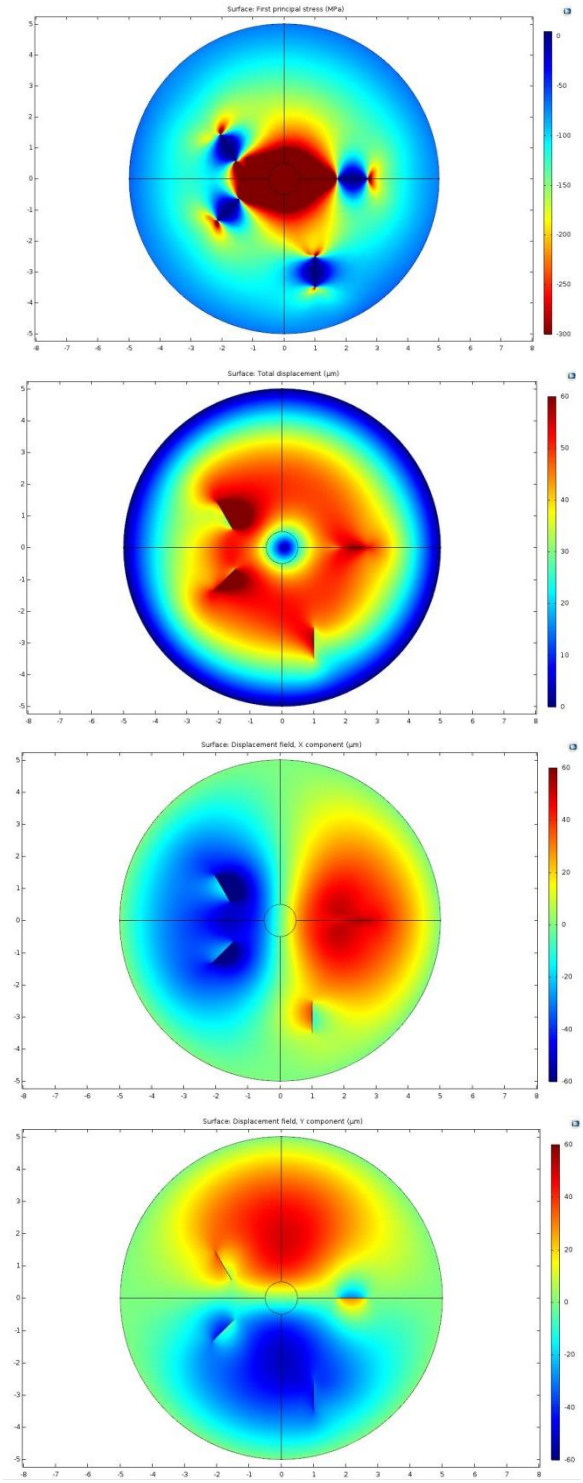

Figure12: plasma torch interaction with limestone specimen in order to induce temperature to create effective thermal stresses to generate new fractures and propagate the existing ones

3. CONCLUSIONS

Plasma torch assisted drilling technique in oil and gas wells with managed pressure condition is discussed. It has challenges including instability of wellbore caused by light drilling fluid, and fracture propagation around the borehole generated by thermal expansion. To resolve these problems some effective gases such as

nitrogen are used as drilling fluids with fewer difficulties. These difficulties can even reduce by dissolving gases in some short film of brine or water. As a consequence one can have a combination so called a foam drilling fluid with low viscosity. The main feature of using such foam is based on the low thermal conductivity of this drilling fluid. It should remind that a large thermal conductivity can easily transfer the plasma torch temperature to the wellbore and this can create some problems including fracture propagation and increasing the skin effect. Thermal operation causes expansion and stresses which can induce many fractures near the borehole. However, the temperature invaded zone may bring advantages such as reduction of the rock strength. Therefore, controlling the heat propagation in the desired direction is a main challenge which can achieve by optimum selection of drilling foam and synchronization of plasma torch interaction with rock textures in order to improve the rate of penetration in hard rocks. As mentioned by effective reduction of the wellbore damage caused by the thermal effect of the torch apparatus and mechanical crashing of the bit, great amount of heat can be conducted to the wellbore. This can cause two possible results: expanding the skin zone by enlarging the melted zone and decreasing the formation damage by the generated thermal fractures.

REFERENCES

J. Zhou, O. N. Stamnes, O. M. Aamo, G. O. Kaasa (2011) Switched Control for Pressure Regulation and Kick Attenuation in a Managed Pressure Drilling System. IEEE Transactions On Control Systems Technology 19:NO 2

G. O. Kaasa, O. N. Stamnes, L. Imsland, O. M. Aamo (2011) simplified hydraulics model used for intelligent estimation of downhole pressure for a managed pressure drilling control system. SPE Drilling & Completion journal 143097

O. Breyholtz, G. Nygaard, M. Nikolaou (2009) managed pressure drilling: using model predictive control to improve pressure control during dual gradient drilling. SPE Drilling & Completion journal 124631

J. M. Godhavn (2009) Control requirements for automatic managed pressure drilling system SPE Drilling & Completion journal 119442

J. E. Gravdal, R. J. Lorentzen, K. K. Fjelde, E. H. Vefring (2005) tuning of computer model parameters in managed pressure drilling applications using an unscented kalman filter technique SPE Journal 97028

Z. Okafor, S. h. Borchardt, G. Akinniranye, T. Bratton, R. Avila, D. Boone (2009) managed pressure drilling using a parasite aerating string. SPE Drilling & Completion journal 119964

Geng Jiaojiao, Yan Jienian, Cao Ming, Bai Xiangshuang, Shi Haimin (2011) Scale deposition mechanism and low-damage underbalanced drilling fluids for high CO2 content gas reservoirs. Petroleum Exploration And Development 38(6):750–755

Zhao Feng, Tang Hongming, Meng Yingfeng, Li Gao, Xing Xijin (2009) Damage evaluation for water-based underbalanced drilling in low-permeability and tight sandstone gas reservoirs. Petroleum Exploration And Development 36(1):113-119

R. Irani, r. Nasimi (2011) application of artificial bee colony-based neural network in bottom hole pressure prediction in underbalanced drilling. journal of petroleum science and engineering 78:6–12

B. Sun, C. Xiang, Z. Wang (2012) influence of altitudes and air humidity to the minimum gas injection rate in air underbalanced drilling. the open petroleum engineering journal 5:104-108

M. Rinne, B. Shen, T. Backers (2013) modeling fracture propagation and failure in a rock pillar under mechanical and thermal loadings. Journal of Rock Mechanics and Geotechnical Engineering 5:73–83

Z. B. Chen, Z. G. Wang, S. J. Zhu (2011) tensile fracture behavior of thermal barrier coatings on super alloy. Surface & Coatings Technology 205:3931-3938

J. Li, F. Song, C. Jiang (2013) direct numerical simulations on crack formation in ceramic materials under thermal shock by using a non-local fracture model. Journal of the European Ceramic Society 33:2677–2687

C. Teodoriu, G. Falcone (2009) Comparing completion design in hydrocarbon and geothermal wells: the need to evaluate the integrity of casing connections subject to thermal stresses. Geothermics 38:238-246

S. Salehi, G. Hareland, K. K. Dehkordi, M. Ganji, M. Abdollahi (2009) casing collapse risk assessment and depth prediction with a neural network system approach. journal of petroleum science and engineering 69:156–162

D. D. Acqua, M. Hodder, T. M. V. Kaiser (2012) burst and collapse responses of production casing in thermal applications SPE Drilling & Completion Journal 151810

A. R. McSpadden, O.D. Cokerr III, G. C. Ruan (2011) advanced casing design with finite element model of effective dogleg severity, radial displacement, and bending loads SPE Drilling & Completion Journal 141458

Coburn JW (1982) Plasma Chem Plasma P 2:1

Sember V, Masˇla´ni A, Krˇenek P, Heinrich M, Nimmervoll R, Pauser H, Hrabovsky´ M (2011) Spectroscopic characterization of a steam arc

cutting torch. Plasma Chem Plasma Process 31:755–770

Peters J, Bartlett B, Lindsay J, Heberlein J (2008) Relating spectroscopic measurements in a plasma cutting torch to cutting performance. Plasma Chem Plasma Process 28:331–352

A. Masˇla´ni, V. Sember, T. Stehrer, H. Pauser (2013) Measurement of Temperature in the Steam Arc jet During Plasma Arc Cutting. Plasma Chem Plasma Process 33:593–604

Johannes Meister, Thomas Arnold (2011) New Process Simulation Procedure for High-Rate Plasma Jet Machining. Plasma Chem Plasma Process 31:91–107

J. Kopecki, D. Kiesler, M. Leins, A. Schulz, M. Walker, M. Kaiser, H. Muegge, U. Stroth (2011) Investigations of a high volume atmospheric plasma torch at 915 MHz. Surface & Coatings Technology 205:S342–S346

K. Bobzin, N. Bagcivan, I. Petkovic (2011) Numerical and experimental determination of plasma temperature during air plasma spraying with a multiple cathodes torch. Journal of Materials Processing Technology 211:1620– 1628

R. T. Lermen, I. G. Machado (2012) Development of a new hybrid plasma torch for materials processing. Journal of Materials Processing Technology 212:2371– 2379

Hoek, E. And Diederichs M.S. (2006) Empirical Estimation of Rock Mass Modulus. International Journal of Rock Mechanics and Mining Sciences 43:203–215

Acknowledgements

The Author is sincerely thanking IGA for their research grant support. And also Weld on Sweden company for their contribution.